mathematics

Article

Numerical Investigation of the Magnetized Reactive Viscous Couple Stress Fluid Flow Down an Inclined Riga Plate with Variable Viscosity

Samuel Olumide Adesanya [1], Tunde Abdulkadir Yusuf [2,*] and Ramoshweu Solomon Lebelo [3]

[1] Department of Mathematical Sciences, Redeemer's University, Ede 232101, Nigeria
[2] Department of Mathematics, Faculty of Science, Adeleke University, Ede 232104, Nigeria
[3] Education Department, Vaal University of Technology, Private Bag X021, Vanderbijlpark 1911, South Africa
* Correspondence: tunde.yusuf@adelekeuniversity.edu.ng

Abstract: Accurate determination of optimum flow and heat transfer condition is one of the major challenges faced in the application of magnetic fluid in the field of medicine and engineering, especially when applied as ferrofluids for targeted drug deliveries, treatment of hyperthermia, sealants in computer hard drives, lubricants in car shafts. In view of these important applications, a mathematical investigation of the flow and heat transfer behavior of reactive magnetic fluids containing nanostructures is presented based on a couple of stress constitutive models. The reactive fluid is assumed to flow through inclined magnetized solid boundaries for energy conversion. The formulation leads to nonlinear coupled equations. The dimensionless equations are numerically solved using the spectral Chebyshev assumed solution for the weighted residual technique, and the correctness of the solution is confirmed using the shooting Runge–Kutta method. The effects of various fluid parameters on velocity, temperature, skin friction, and heat transfer rates are described in tabular and graphical form, along with suitable physical explanations. Thermal analysis computations are also presented. According to the findings, an enhanced couple of stress fluid and variable viscosity parameters reduced the skin drag and heat transfer rate at the bottom wall. Furthermore, the thermal stability of the flow can be achieved with increasing values modified Hartman number while increasing couple stress parameter encourages thermal instability in the flow domain.

Keywords: reactive magnetic fluid; couple stress; Riga surface; Chebyshev spectral method

MSC: 76D99; 76W99

Citation: Adesanya, S.O.; Yusuf, T.A.; Lebelo, R.S. Numerical Investigation of the Magnetized Reactive Viscous Couple Stress Fluid Flow Down an Inclined Riga Plate with Variable Viscosity. *Mathematics* **2022**, *10*, 4713. https://doi.org/10.3390/math10244713

Academic Editors: Efstratios Tzirtzilakis and Mario Versaci

Received: 11 November 2022
Accepted: 9 December 2022
Published: 12 December 2022

1. Introduction

The biomedical and rheological properties of ferrofluids have recently been widely studied. This is due to their applications in some areas of medicine and engineering [1–3]. Regarding real-world applications, the bulk of ferrofluids has non-Newtonian properties. The couple stress fluid is one of the most well-known non-Newtonian fluid models. The theory of couple stress is a broad notion of viscous fluid that allows for polar effects like the presence of couple stresses and body couples in classical theory. Couple stress fluids have a high viscosity and polar effects (Abbas et al. [4]). This is first considered by Stokes [5] and has been an area of potential interest in many physical and engineering processes. Hence, the study of flow and heat transfer analysis of couple stress fluid has captured the mind of several researchers [6–9]. The work in [4] examines the mixed convection flow of an electrically conducting couple stress fluid in an inclined channel. They noticed a reduction in the thermal field as the channel was tilted. The concept of channel flow having non-zero inclination has been instrumental in diverse industrial processes such as chemical processing, iron removal, and electrical system. Because of its applications, Sui et al. [10] examined the behavior of physical components on non-Newtonian fluid flow past an inclined surface. RamReddy et al. [11] reported the nonlinear convective flow of non-Newtonian liquid over an inclined porous regime. Significant change is observed as the angle of inclination is improved. Yusuf et al. [12] also presented a semi-analytical solution on a micropolar fluid flow over an inclined geometry with velocity slip. Very recently, Ahmad et al. [13] analytically examined Stoke's theory of couple stress fluid over an inclined channel under variable viscosity.

To improve the fluid thermophysical characteristics of some industrial liquids that are poor conductors of electricity, an external device known as a Riga plate is introduced to enhance the heat transfer attributes. Riga plate is an array of a magnetic bar supported by permanent magnets and alternating electrons. It could also act as an external device to boost fluid electricity. Gailitis and Lielausis [14] built a Riga plate under the influence of magnetic and electrical fields that generate a Lorentz force along the wall, which helps to control fluid flow. Given this, several researchers have discussed laminar flow under the influence of magnetic force along the Riga surface under various geometries afterward [15–18]. Nadeem et al. [19] studied the slip effect on a rotation fluid over a Riga channel. They discovered that the momentum boundary layer thickness declined due to the Riga surface. Naseem et al. [20] examined a grade three fluid flow with the influence of Cattaneo-Cristov heat flux over a Riga surface. Recently, stagnation point fluid flow and heat transfer over a vertical surface consisting of magnetic electrodes have been investigated by Khashi'ie et al. [21]. They indicated a diminution in the heat transfer rate due to an upsurge in the magnet and electrode width. Furthermore, fluid physical properties are affected by temperature changes. Previous heat conduction research relied heavily on the ambient fluid's unchanging physical properties. However, certain qualities, remarkably fluid viscosity, are known to alter with temperature. It is vital to account for the temperature-dependent fluctuation of viscosity in order to effectively describe flow and heat transfer rates. In this regard, the influence of temperature-dependent viscosity on a transient flow along a slanted surface is examined by Chinyoka et al. [22]. Further, Nadeem et al. [23] discussed nanofluid flow with magnetic and variable viscosity effects over a curved surface. They further established that thermal distribution declined for augmenting variable viscosity. Megahed et al. [24] considered the slip effect on a viscoelastic fluid flow over a surface with variable viscosity.

Except for a few problems, numerical algorithms have proven to be useful in solving continuum mechanics problems in which flow and heat transport are approximated by highly nonlinear differential equations. This typically results in the issue of convergence and computational time. Several approximate methods have become enormously popular in solving nonlinear models. However, of interest is the Chebyshev spectral collocation method. The main advantage of these methods lies in their accuracy for a given number of unknowns. For problems whose solutions are sufficiently smooth, they exhibit exponential convergence/spectral accuracy rates as in Mai-Duy and Tanner [25]. For instance, the method's efficiency is described in some different kinds of nonlinear partial differential equations by Khater et al. [26]. Comprehensive discussions on Chebyshev spectral collocation methods are available in different review articles [27–29]. The investigations mentioned above have demonstrated reactive flow along the Riga surface, but they have yet to examine how reactive fluid flow is across a Riga channel. This investigation will address this gap and offer a thorough understanding of fluid flow through heated, magnetic boundaries. As a result, three areas are the focus of our attention: first, the flow of a reactive couple stress fluid in incline walls with temperature-dependent viscosity; second, the impact of the fluid reactiveness through a magnetized heated channel; and third, the analysis of the numerical solution using a reliable solution technique. The Solutions to the nonlinear ODEs are generated via the Chebyshev spectral collocation technique, and results are displayed through graphs. Further, the solution compared with a different numerical scheme is also presented to corroborate our results.

2. Model Formulation

This paper establishes a continuous incompressible flow and heat transfer of a temperature-dependent reactive couple stress fluid in a non-porous inclined Riga plate. As demonstrated by the flow geometry (see Figure 1), the (x, y) Cartesian coordinate is chosen along the plates so that the x-axis is parallel to the flow and the y-axis is perpendicular to it. The plates are at an angle M to the horizontal. Furthermore, when considering a gravity-driven steady flow, the fully evolved incompressible fluid implies $V = (u(y),0,0)$, $T = T(y)$, as indicated in the flow geometry. The governing equations for this problem are based on the Cartesian system for continuity, momentum, and energy equations as follows:

$$\nabla.V = 0 \tag{1}$$

$$\rho \frac{DV}{Dt} = \nabla\tau - \eta\nabla^4 V + \rho f + \mathrm{J} \times \mathrm{B} \tag{2}$$

$$\rho C_P \frac{DT}{Dt} = k\nabla^2 T + \tau L \ + QAC_0 e^{-\frac{E}{RT}} \tag{3}$$

In Equations (1)–(3), V represents the velocity vector, ∇ is the grad operator, (ρ, C_P, t, T) —represents the fluid density, specific heat, time, and fluid temperature, respectively, $\left(k, \tau, L, \frac{D}{Dt}\right)$ are the thermal conductivity of the fluid, Cauchy stress tensor, the gradient of the velocity vector and material derivative. $(\eta, f, \mathrm{J}, \mathrm{B})$—couple stress coefficient, body force, the current density of electric field and a sum of the magnetic field, (Q, A, C_0), (E, R), Q—the heat of reaction, A—rate constant, C_0 initial reactant concentration, E—activation energy, R—universal gas constant,
where

$$\tau = -PI + \mu A_1,\ A_1 = L + L^T,\ \frac{D(*)}{Dt} = \frac{\partial(*)}{\partial t} + v.\nabla(*) \tag{4}$$

are the formal definitions of the Cauchy tensor, the First Rilivin–Ericksen tensor, and the material derivative.

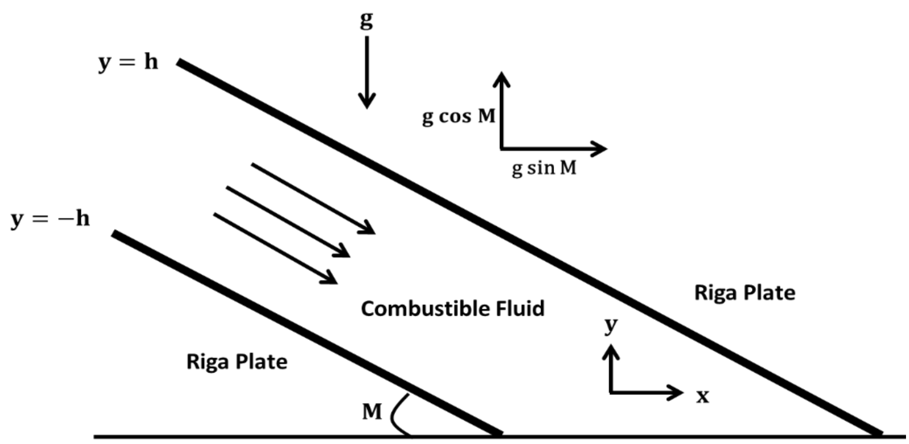

Figure 1. Flow Channel.

Using the Ginsberg approximation, then the Lorentz force is expressed as

$$\mathrm{J} \times \mathrm{B} \approx \sigma(E \times \mathrm{B}) = \frac{\pi}{8} J_0 M_0 e^{-\frac{\pi}{T} y'} \tag{5}$$

Given the combustible fluid assumptions, Equations (1)–(3) can be written as

$$\frac{\partial u'}{\partial x'} = 0 \tag{6}$$

$$0 = -\frac{dp}{dx} + \frac{d}{dy'}\left(\mu'\frac{du'}{dy'}\right) - \eta\frac{d^4u'}{dy'^4} + \rho g\cos M + \frac{\pi}{8}J_0M_0e^{-\frac{\pi}{l}y'} \tag{7}$$

$$0 = k\frac{d^2T}{dy'^2} + \mu'\left(\frac{du'}{dy'}\right)^2 + \eta\left(\frac{d^2u'}{dy'^2}\right)^2 + QAC_0e^{-\frac{E}{RT}} \tag{8}$$

Together with the boundary conditions

$$u'(\pm h) = 0 = \frac{d^2u'}{dy'^2}(\pm h),\ T(\pm h) = T_0 \tag{9}$$

The inverse relationship between fluid temperature and temperature is a well-known phenomenon in the literature

$$\mu' = \mu_0e^{-\alpha'(T-T_0)} \cong \mu_0\big(1-\alpha'(T-T_0)\big) \tag{10}$$

Since viscosity variation temperature is usually, i.e., $0 < \alpha' << 1$. To make Equations (7)–(9) dimensionless, we introduce the following dimensionless variables and parameters

$$\begin{gathered} y = \frac{y'}{h},\ u = \frac{\mu_0u'}{\rho gh^2\cos M},\ H^2 = \frac{\pi J_0M_0}{8\rho g\cos M}, \beta^2 = \frac{\mu_0h^2}{\eta},\ \gamma = \frac{\pi h}{l},\ \theta = \frac{E(T-T_0)}{RT_0^2}, Nu = \frac{hEq_w}{kRT_0^2} \\ \alpha = \frac{\alpha' RT_0^2}{E}, \lambda = \frac{QEAh^2C_0e^{-\frac{E}{RT_0}}}{T_0^2RK},\ \varepsilon = \frac{RT_0}{E},\ \delta = \left(\frac{\rho g\cos M}{h}\right)^2\frac{e^{\frac{E}{RT_0}}}{QC_0Ah^2}, C_F = \frac{\mu_0\tau_w}{h\rho g\cos M}. \end{gathered} \tag{11}$$

So that the dimensionless form of (7)–(9) becomes:

$$0 = 1 + \frac{d}{dy}\left((1-\alpha\theta)\frac{du}{dy}\right) - \frac{1}{\beta^2}\frac{d^4u}{dy^4} + H^2e^{-\gamma y};\ u(\pm 1) = 0 = \frac{d^2u}{dy^2}(\pm 1) \tag{12}$$

$$0 = \frac{d^2\theta}{dy^2} + \lambda\left(e^{\frac{\theta}{1+\varepsilon\theta}} + \delta(1-\alpha\theta)\left(\frac{du}{dy}\right)^2 + \frac{\delta}{\beta^2}\left(\frac{d^2u}{dy^2}\right)^2\right);\quad \theta(\pm 1) \tag{13}$$

The shear stress at the wall τ_w and heat flux q_w are respectively expressed as

$$\tau_w = \mu'\frac{du'}{dy'} - \eta\frac{d^3u'}{dy'^3}\bigg|_{y'=-h} \quad \text{and} \quad q_w = -k\frac{dT}{dy'}\bigg|_{y'=-h} \tag{14}$$

Using Equation (11) in (14), we get

$$S_F = (1-\alpha\theta)\frac{du}{dy} - \frac{1}{\beta^2}\frac{d^3u}{dy^3}\bigg|_{y=-1}, \qquad Nu = -\frac{d\theta}{dy}\bigg|_{y=-1} \tag{15}$$

3. Spectral Chebyshev Collocation Method of Solution

In view of the nonlinear nature of the model, Equations (12) and (13) are numerically solved. A collocation method based on the Chebyshev polynomial is remarkable and instrumental in addressing the solution to the boundary value problem. The numerical solutions obtained in $[-1, 1]$ are expanded as a finite series in Chebyshev polynomial expressed as

$$u(y) \approx u^{Np}(y) = \sum_{i=0}^{Np} a_nT_n(y),\ \text{and}\ \ \theta(y) \approx \theta^{Np}(y) = \sum_{i=0}^{Np} b_nT_n(y) \tag{16}$$

where $\{a_n\}_{n=0}^{Np}$ and $\{b_n\}_{n=0}^{Np}$ are sets of expansion coefficients to be determined. Now, substituting $u^n(y)$ and $\theta^n(y)$ in Equations (12) and (13) yields the residual approximation of the form:

$$R_1(y) = 1 + \left(\left(1 - \alpha\theta^{Np}\right)u_y^{Np}\right)' - \frac{1}{\beta^2}u_{y,y,y,y}^{Np} + Ha^2 e^{-\gamma y}, \tag{17}$$

$$R_2(y) = \theta_{y,y}^{Np} + \lambda\left(e^{\frac{\theta^{Np}}{1+\varepsilon\theta^{Np}}} + \delta\left(1 - \alpha\theta^{Np}\right)\left(u_y^{Np}\right)^2 + \frac{\delta}{\beta^2}\left(u_{y,y}^{Np}\right)^2\right) \tag{18}$$

the approximation formula must be exact at y equal to y_i by the transformed zeros of the Chebyshev Gauss- Lobato collocation nodes to $[-1, 1]$.

$$y_i = \left(-\cos\left(\frac{i\pi}{Np}\right)\right), \quad i = 0, 1, 2, \ldots, Np \tag{19}$$

The relation

$$R_1(y_i) = 0, \text{ and } R_2(y_i) = 0, \quad i = 0, 1, 2, \ldots, Np \tag{20}$$

must be established. The rth-order derivative of the variables is then yielded through differentiation as

$$\frac{d^r u}{dy^r} = \sum_{n=0}^{Np} a_n \frac{d^r T_n}{dy^r} \text{ and } \frac{d^r \theta}{dy^r} = \sum_{n=0}^{Np} b_n \frac{d^r T_n}{dy^r} \tag{21}$$

The values of the derivative with $n = 1, 2, \ldots, r$ at the Gauss–Lobatto can be evaluated by

$$\begin{array}{ccc} \frac{d\widehat{u}}{dy} = D^{(1)}\widehat{u} = D\widehat{u} & & \frac{d\widehat{\theta}}{dy} = D^{(1)}\widehat{\theta} = D\widehat{\theta} \\ \frac{d^2\widehat{u}}{d^2y} = D^{(2)}\widehat{u} = D^2\widehat{u} & \text{and} & \frac{d^2\widehat{\theta}}{d^2y} = D^{(2)}\widehat{\theta} = D^2\widehat{\theta} \\ \cdots\ \cdots\ \cdots\ \cdots & & \cdots\ \cdots\ \cdots\ \cdots \\ \frac{d^r\widehat{u}}{d^ry} = D^{(r)}\widehat{u} = D^r\widehat{u} & & \frac{d^r\widehat{\theta}}{d^ry} = D^{(r)}\widehat{\theta} = D^r\widehat{\theta} \end{array} \tag{22}$$

where $\widehat{u} = \left(u(y_0), u(y_1), \ldots, u(y_{Np})\right)^T$ and $\widehat{\theta} = \left(\theta(y_0), \theta(y_1), \ldots, \theta(y_{Np})\right)^T$ are the vectors, $D^{(\bullet)}$ are the differential matrices. Using (16), the ordinary differential equations are reduced to systems of algebraic equations. For the sake of validation, Equations (12) and (13) are also solved iteratively via the Runge–Kutta–Fehlberg (RKF) integration technique. This computation is carried out on a computer symbolic package. The RKF is introduced to guarantee the accuracy of the present method.

4. Results and Discussion

In this section, the solutions obtained using Chebyshev polynomial as an admissible trial function for the nonlinear problem are displayed graphically and explained for the profile of velocity, the temperature distributions, the coefficient of skin friction, and the local Nusselt number are presented for various emerging parameters. Tabular results are also presented for comparison in Tables 1–3. In Tables 4 and 5, stability analysis and convergence results are displayed. Table 1 establishes the correctness of the spectral collocation method when compared with its exact solution. The uniqueness of the solution is confirmed since $\alpha << 1$ is infinitely small. Therefore, the Chebyshev trial function provides a very good approximation for the uncoupled problem. Moreover, for the Coupled system when $\alpha \neq 0$, tables for the comparison of the numerical solutions by spectral collocation and the Runge–Kutta–Fehlberg (RKF) integration technique are presented for Equations (12) and (13). In Tables 2 and 3, the error ranges from $10^{-17}$and 10^{-8} for Equation (12) which means that the two results converge to one. The error range for the solution of (13) is $10^{-18}$and 10^{-8}. Therefore, there is a perfect agreement between the two numerical solutions; as a result, the approximation is okay. Table 4 represents the influence of flow parameters on the wall friction and heat transfer rate. The result revealed that increasing values of the viscous dissipation parameter reduces the wall skin friction while it increases the wall Nusselt number. This is true due to the irreversible work done in converting kinetic energy to heat energy. Furthermore, the Nusselt number increases due to decreasing heat transfer by conduction across the channel width.

Moreover, magnets and electrodes at the solid boundaries increase the skin friction and the wall Nusselt number. This shows that flow resistance and rate of heat transfer at the wall become higher with the increasing values of the modified Hartmann number. Similar behavior is noticed with increasing couple stress inverse parameters. Finally, increasing values of the viscosity variation parameter show that momentum transfer from the laminar flow to the wall increases with the variation of the viscosity parameter. Table 5 shows the flow parameters' effect on the flow's thermal stability. The result shows that the activation energy parameter increases the critical values, thus stabilizing the flow. The contribution of the modified Hartman number is seen to encourage thermal instability in the flow. This is correct physically since the magnetic term increases the fluid temperature. It is expected to encourage thermal runaway in the flow domain. A similar explanation holds for the viscosity variation parameter and the inverse of the couple stress parameter in terms of encouraging thermal instability in the flow domain. In Table 6, the convergence of the Chebyshev series is obtained when the number of terms in the approximating polynomial is 10 for the given parameter values.

Table 1. Comparison of Exact solution and Numerical solution when $\alpha = 0$, $\beta = 0.1$, $H = 1$, $\gamma = 1$.

y	Exact	SCM	Absolute Error
-1	$-5.03992583264522 \times 10^{14}$	0.000000000000000000	$5.039925832645223 \times 10^{14}$
-0.75	0.0017454436901435553	0.001745454926416422	$1.123627286700457 \times 10^{-8}$
-0.5	0.003173227582038684	0.003173231306211247	$3.724172563217276 \times 10^{-9}$
-0.25	0.004076000485437167	0.004076004401859833	$3.916422666207231 \times 10^{-9}$
0	0.0043502281691282264	0.004350231164298437	$2.995170210809417 \times 10^{-9}$
0.25	0.003981732876595737	0.003981735066616083	$2.190020346494459 \times 10^{-9}$
0.5	0.0030344730267644108	0.003034472001333134	$1.025431276783367 \times 10^{-9}$
0.75	0.0016418517123099419	0.001641848839780530	$2.872529411600613 \times 10^{-9}$
1	$4.46751760135205 \times 10^{-14}$	$-4.910861206864707 \times 10^{-9}$	$4.910905882040721 \times 10^{-9}$

Table 2. Validation of result of Equation (12) when $\delta = \beta = \gamma = H = 1$, $\lambda = \varepsilon = \alpha = 0.1$.

y	$u(y)_{SCM}$	$u(y)_{RK4}$	$\lvert u(y)_{SCM} - u(y)_{RK4} \rvert$
-1	1.35477×10^{-17}	0.000000	1.35477×10^{-17}
-0.75	0.126368	0.126368	3.73265×10^{-9}
-0.50	0.228617	0.228617	7.89402×10^{-10}
-0.25	0.292212	0.292212	1.68506×10^{-9}
0.0	0.310659	0.310659	1.45745×10^{-9}
0.25	0.283667	0.283667	1.01772×10^{-10}
0.50	0.216004	0.216004	3.25084×10^{-9}
0.75	0.116914	0.116914	8.42008×10^{-9}
1	-7.58235×10^{-19}	1.41621×10^{-8}	1.41621×10^{-8}

Table 3. Validation of result of Equation (13) when $\delta = \beta = \gamma = H = 1$, $\lambda = \varepsilon = \alpha = 0.1$.

y	$\theta(y)_{WRM}$	$\theta(y)_{RK4}$	$\lvert \theta(y)_{WRM} - \theta(y)_{RK4} \rvert$
-1.0	-2.32225×10^{-18}	0.0000000	2.32225×10^{-18}
-0.75	0.0333263	0.0333263	6.36403×10^{-9}
-0.50	0.0578145	0.0578142	6.82415×10^{-9}
-0.25	0.0725453	0.0725453	6.93838×10^{-9}
0.0	0.0770979	0.0770979	1.05644×10^{-8}
0.25	0.0715674	0.0715674	1.21143×10^{-8}
0.50	0.0564163	0.0564163	1.43481×10^{-8}
0.75	0.0323197	0.0323197	1.81587×10^{-8}
1.0	-2.63179×10^{-19}	-2.03698×10^{-8}	2.03698×10^{-8}

Table 4. Skin Friction and Nusselt number for various fluid parameters.

H	δ	ε	λ	α	β	γ	S_F	Nu
1	1	0.3	0.5	0.1	1	1	2.54320	0.89053
1	2	0.3	0.5	0.1	1	1	2.54319	1.17403
1	3	0.3	0.5	0.1	1	1	2.54318	1.46102
2	1	0.3	0.5	0.1	1	1	7.17259	2.58254
3	1	0.3	0.5	0.1	1	1	14.8866	9.30193
1	1	0.3	0.5	0.1	2	1	2.54350	1.20465
1	1	0.3	0.5	0.1	3	1	2.54385	1.36500
1	1	0.3	0.5	0.2	1	1	2.54333	0.89233
1	1	0.3	0.5	0.3	1	1	2.54345	0.89417

Table 5. Computation of Critical values of Frank–Kameneskii parameter.

δ	ε	α	β	γ	H	λ_C
1	0.1	0.1	1	1	1	0.861553
1	0.2	0.1	1	1	1	1.046770
1	0.3	0.1	1	1	1	1.838140
1	0.1	0.1	1	1	2	0.560669
1	0.1	0.1	1	1	3	0.305436
1	0.1	0.2	1	1	1	0.858432
1	0.1	0.3	1	1	1	0.855150
1	0.1	0.1	2	1	1	0.793590
1	0.1	0.1	3	1	1	0.778710

Table 6. Rapid convergence of the Spectral Weighted Residual Method.

N	δ	ε	α	β	γ	H	λ_C
5	1	0.1	0.1	1	1	1	0.961880
10	1	0.1	0.1	1	1	1	0.861512
15	1	0.1	0.1	1	1	1	0.861553
20	1	0.1	0.1	1	1	1	0.861553
25	1	0.1	0.1	1	1	1	0.861553
30	1	0.1	0.1	1	1	1	0.861553

Figure 2 relates the influence of the viscosity variation parameter on the velocity profile. The graphical result shows that flow velocity rises with increasing value of the viscosity variation parameter, showing that viscous fluid becomes lighter with thermal effect. In other words, the heat transfer to the fluid from an exothermic chemical reaction has a thinning effect on the fluid viscosity. In Figure 3, the effect of the viscosity variation parameter on the temperature distribution within the flow channel is presented. The result shows that the viscosity parameter increases the maximum temperature. This effect is directly connected with the irreversible energy conversion from kinetic to heat. The effect of nanoparticles on the flow and thermal distribution is displayed n Figures 4 and 5. These nanoparticles could present as drugs for a specific treatment, polymer additives to enhance the fluid rheological properties of some lubricants, etc. As these nano-sized particles are added, internal friction is created, and the velocity of the fluid decreases, as shown in the inverse of the couple stress parameter. Evidently, as the fluid thickens, inter-molecular interaction declines. This is also associated with a decline in fluid temperature as observed in the plot of temperature distribution with couple stress inverse.

Figures 6 and 7 demonstrate the impact of modified Hartmann number (H) on both velocity and temperature distributions, respectively. It is noticed in Figure 6 that an improvement in the velocity profile occurred as the modified Hartmann number (H) increased. This is because the external magnetic field strengthens as the values of the modified Hartmann number (H) become more significant, consequently improving the flow motion. This is a well-behaved solution since $+H^2 e^{\eta y}$ represents a positive definite function as used in Equation (12) for all values of $Ha, \ \eta$. Moreover, increasing the same parameter (H) leads to an upsurge in temperature distribution. This effect can be seen in the momentum transfer through viscous dissipation, which acts as a heat source in the flow domain, as seen in Figure 7.

The influence of the velocity and temperature field against the Frank–Kameneskii parameter (λ) is displayed in Figures 8 and 9, respectively. The emerged parameter results from the Arrhenius kinetics that releases energy from heat into the fluid stream. As depicted in Figure 8, an increment in the Frank–Kameneskii parameter is noticed to enhance flow velocity. This is physically correct due to the heat of the reaction that produces a melting effect on the viscous fluid. The thinning effect guarantees enhanced flow down the inclined channel. The exothermic nature of the Arrhenius kinetics is seen to increase the temperature distribution as the Frank–Kameneskii parameter (λ) value increases, as shown in Figure 9. The diagram for the bifurcation slice that is typical of all laminar flames in combustion problems is illustrated in Figure 10. This shows the effect of the maximum temperature against the Frank–Kameneskii parameter (λ). In the region I and II where $\lambda_c < 0.861553$ two values of λ exist for the maximum temperature. Only one solution exists at the point when $\lambda_c = 0.861553$ while no solution is possible beyond $\lambda_c > 0.861553$ where heat generation is far greater than heat dissipation, this corresponds to the hazardous blow-up point where spontaneous ignition occurs. Accurate determination of critical values is vital in ensuring the safety of lives and properties

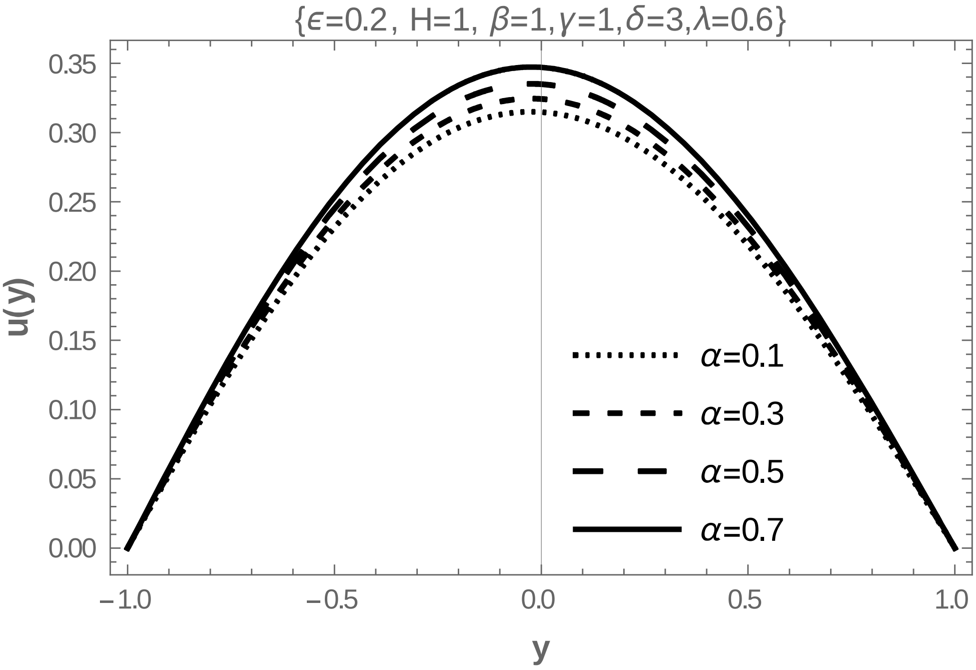

Figure 2. Velocity profile with viscosity variation parameter (α).

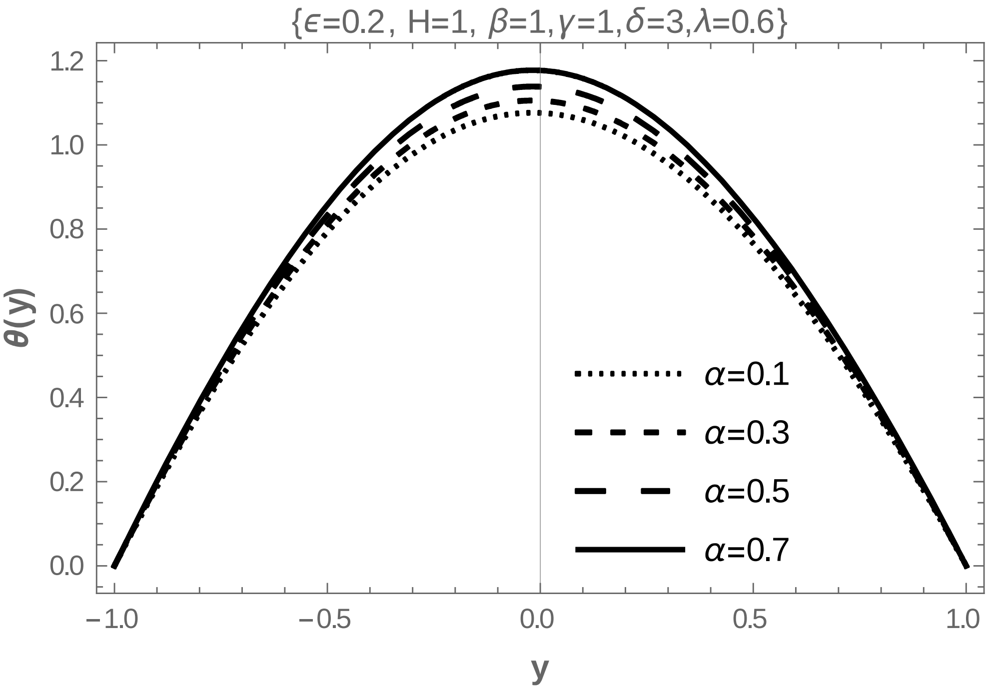

Figure 3. Thermal distribution with viscosity variation parameter (α).

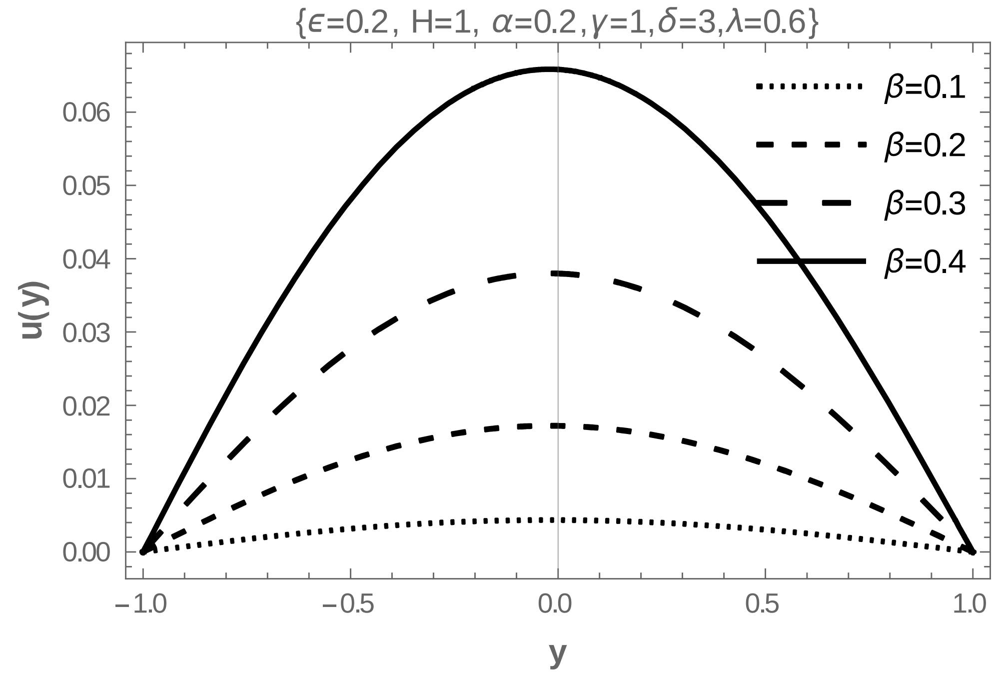

Figure 4. Velocity profile with couple stress inverse parameter (β).

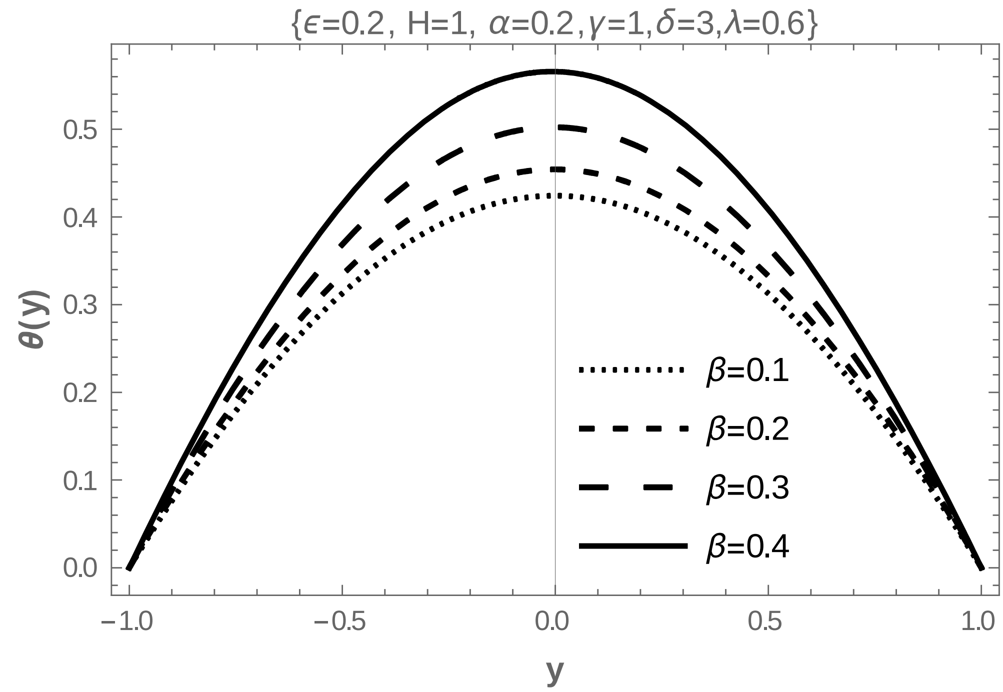

Figure 5. Temperature distribution with couple stress inverse parameter (β.

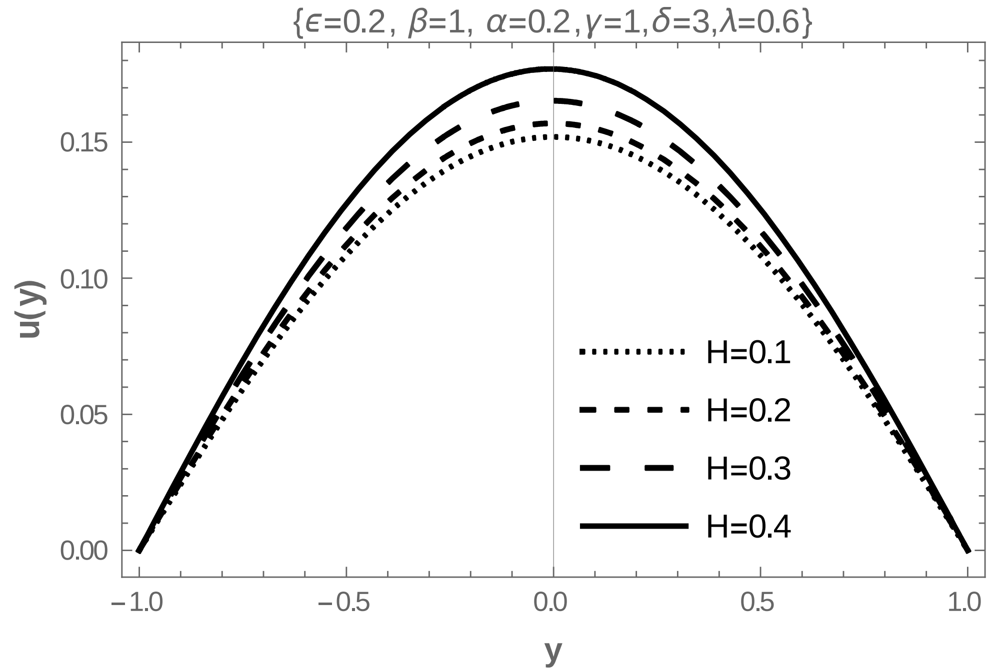

Figure 6. Velocity profile with modified Hartman number (H).

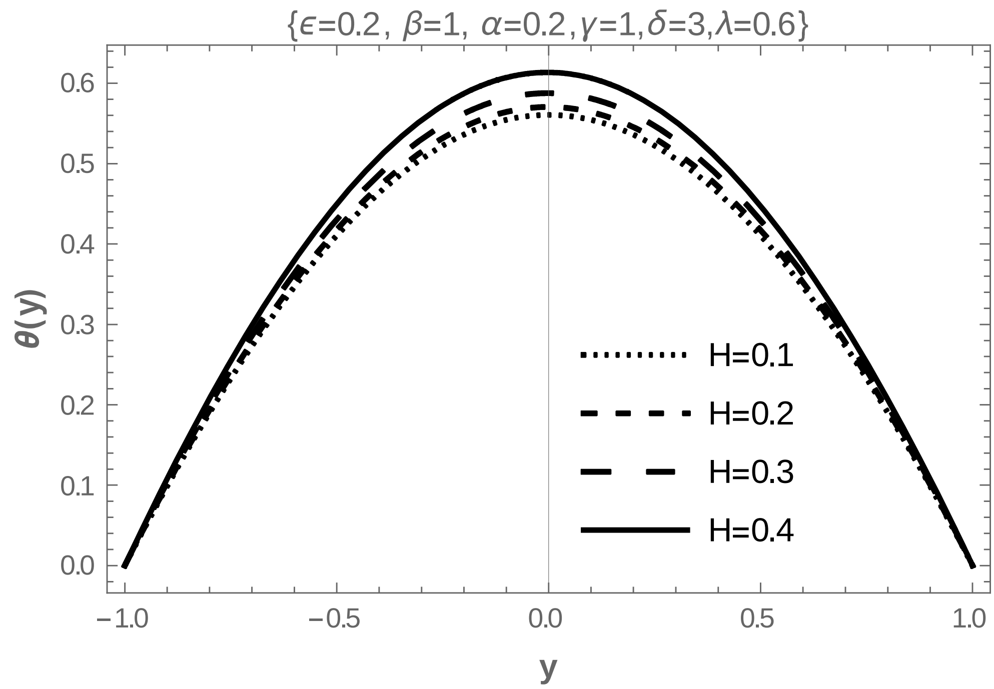

Figure 7. Temperature distribution with modified Hartman number (H).

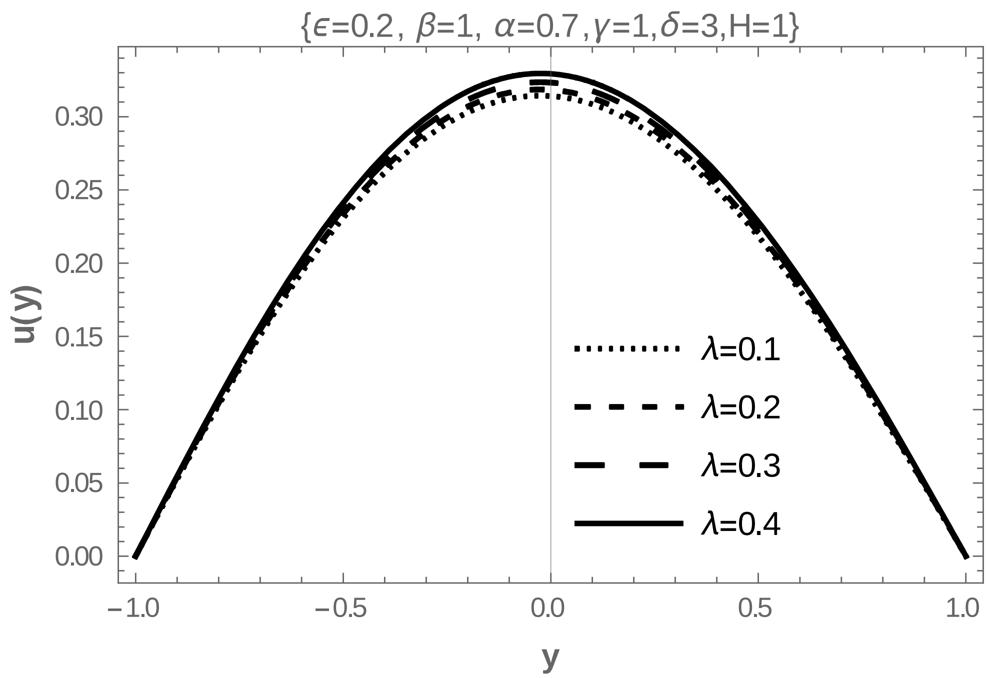

Figure 8. Velocity profile with Frank–Kameneskii parameter (λ).

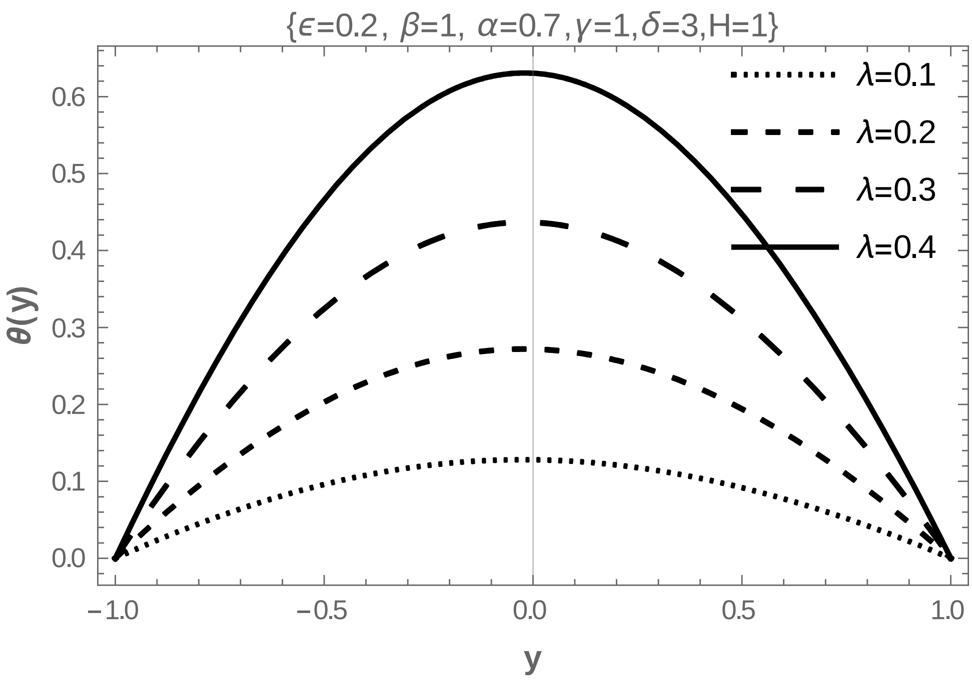

Figure 9. Temperature distribution with Frank–Kameneskii parameter (λ).

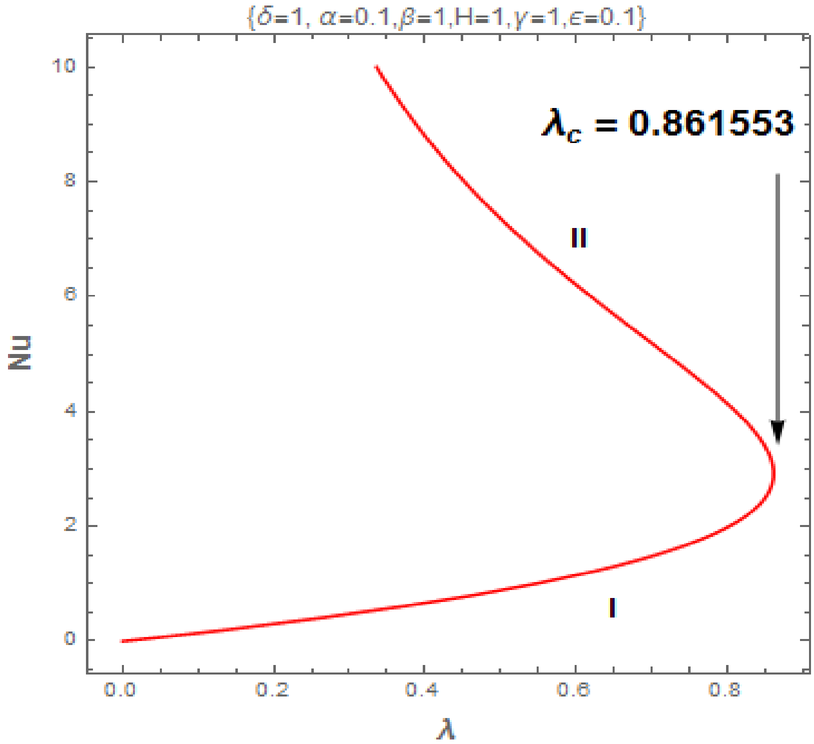

Figure 10. Bifurcation slice.

5. Conclusions

A mathematical model of a magnetized reactive variable viscous couple stress fluid flow down an inclined Riga plate has been investigated. Solutions are obtained numerically using the spectral collocation technique. Runge–Kutta–Fehlberg (RKF) integration technique is additionally employed in the model to validate the spectral collocation method. Tables and graphical results are available and analyzed. The significant outcomes of this current investigation are as follows:

- The fluid motion strengthened with an increase in the modified Hartman number and the couple stress parameter.
- As the fluid viscosity varies, the fluid motion and the heat balance enhance along the inclined channel.
- Large values of the Frank–Kameskii parameter significantly boost the thermal field. Also, the flow becomes thermal stable with an activation energy parameter increase.
- The velocity gradient at the lower wall increases for larger values of modified Hartman and couple stress parameters while slightly dropping for increasing values of the viscous heating parameter.
- At the lower wall, the heat transfer rate dramatically improves as the values of modified Hartman, viscous heating, and couple stress parameters enhance.

Author Contributions: Conceptualization, S.O.A.; Data curation, T.A.Y.; Formal analysis, S.O.A. and R.S.L.; Funding acquisition, R.S.L.; Investigation, T.A.Y.; Methodology, S.O.A.; Project administration, R.S.L.; Resources, T.A.Y.; Software, S.O.A.; Writing original draft, S.O.A. All authors have read and agreed to the published version of the manuscript.

Funding: This research received no external funding.

Conflicts of Interest: The authors declare no conflict of interest.

Nomenclature

M	Inclination angle of channel
M_0	magnetization of the magnets
J_0	applied current density in the electrodes
g	acceleration due to gravity
H^2	modified Hartman number
Q	heat of reaction
A	rate constant
C_0	initial concentration of the reactant species
E	activation energy
R	universal gas constant
T	fluid temperature [K]
K	thermal conductivity [$\mathrm{Wm}^{-1}\ \mathrm{K}^{-1}$]
l	magnets and electrodes width
u', u	dimensinal and dimensionless velocity [ms^{-1}]
h	channel width [m]
x, y	Cartesian coordinates [m]
p	fluid pressure
T_0	geometry wall temperature
Greek	
μ'	dynamic viscosity [Pas]
μ_0	viscosity constant
σ	electrical conductivity
ρ	density of the fluid [kgm^{-3}]
α	temperature-dependent viscous parameter
α'	temperature-dependent viscous parameter
β	couple stress parameter
θ	dimensionless temperature
γ	dimensionless parameter
λ	Frank–Kameneskii parameter
ε	activation energy parameter,
δ	viscous heating parameter
η	coefficient of couple stress

References

1. Odenbach, S. Recent progress in magnetic fluid research. *J. Phys. Condens. Matter* **2004**, *16*, R1135–R1150. [CrossRef]
2. Kozissnik, B.; Bohórquez, A.; Dobson, J.; Rinaldi, C. Magnetic fluid hyperthermia: Advances, challenges, and opportunity. *Int. J. Hyperth.* **2013**, *29*, 706–714. [CrossRef] [PubMed]
3. Rinaldi, C.; Chaves, A.; Elborai, S.; He, X.; Zahn, M. Magnetic fluid rheology and flows. *Curr. Opin. Colloid Interface Sci.* **2005**, *10*, 141–157. [CrossRef]
4. Abbas, Z.; Hasnain, J.; Sajid, M. Hydromagnetic Mixed Convective Two-Phase Flow of Couple Stress and Viscous Fluids in an Inclined Channel. *Z. Nat. A* **2014**, *69*, 553–561. [CrossRef]
5. Stokes, V.K. Couple stresses in fluids. *Phys. Fluids* **1966**, *9*, 1709–1715. [CrossRef]
6. Hayat, T.; Aziz, A.; Muhammad, T.; Ahmad, B. Influence of Magnetic Field in Three-Dimensional Flow of Couple Stress Nanofluid over a Nonlinearly Stretching Surface with Convective Condition. *PLoS ONE* **2015**, *10*, e0145332. [CrossRef]
7. Makinde, O.D.; Eegunjobi, A.S. Entropy Generation in a Couple Stress Fluid Flow Through a Vertical Channel Filled with Saturated Porous Media. *Entropy* **2013**, *15*, 4589–4606. [CrossRef]
8. Adesanya, S.O.; Makinde, O.D. Effects of couple stresses on entropy generation rate in a porous channel with convective heating. *Comput. Appl. Math.* **2015**, *34*, 293–307. [CrossRef]
9. Tripathi, D.; Yadav, A.; Beg, O.A. Electro-osmotic flow of couple stress fluids in a micro-channel propagated by peri-stalsis. *Eur. Phys. J. Plus* **2013**, *132*, 173. [CrossRef]
10. Sui, J.; Zheng, L.; Zhang, X.; Chen, G. Mixed convection heat transfer in power law fluids over a moving conveyor along an inclined plate. *Int. J. Heat Mass Transf.* **2015**, *85*, 1023–1033. [CrossRef]
11. RamReddy, C.; Naveen, P.; Srinivasacharya, D. Nonlinear Convective Flow of Non-Newtonian Fluid over an Inclined Plate with Convective Surface Condition: A Darcy–Forchheimer Model. *Int. J. Appl. Comput. Math.* **2018**, *4*, 51. [CrossRef]
12. Yusuf, T.; Kumar, R.N.; Prasannakumara, B.; Adesanya, S. Irreversibility analysis in micropolar fluid film along an incline porous substrate with slip effects. *Int. Commun. Heat Mass Transf.* **2021**, *126*, 105357. [CrossRef]

13. Ahmad, F.; Nazeer, M.; Ali, W.; Saleem, A.; Sarwar, H.; Suleman, S.; Abdelmalek, Z. Analytical Study on Couple Stress Fluid in an inclined Channel. *Sci. Iran.* **2021**, *28*, 2164–2175. [CrossRef]
14. Gailitis, A.; Lielausis, O. On a possiblilty to reduce the hydrodynamical resistance of a plate in an electrolyte. *Appl. Magnetohydrodyn.* **1961**, *12*, 143–146.
15. Zaib, A.; Haq, R.U.; Chamkha, A.J.; Rashidi, M.M. Impact of partial slip on mixed convective flow towards a Riga plate comprising micropolar TiO_2-kerosene/water nanoparticles. *Int. J. Numer. Methods Heat Fluid Flow* **2019**, *29*, 1647–1662. [CrossRef]
16. Nayak, M.; Shaw, S.; Makinde, O.D.; Chamkha, A.J. Investigation of Partial Slip and Viscous Dissipation Effects on the Radiative Tangent Hyperbolic Nanofluid Flow Past a Vertical Permeable Riga Plate with Internal Heating: Bungiorno Model. *J. Nanofluids* **2019**, *8*, 51–62. [CrossRef]
17. Nadeem, S.; Malik, M.Y.; Abbas, N. Heat transfer of three-dimensional micropolar fluid on a Riga plate. *Can. J. Phys.* **2019**, *98*, 32–38. [CrossRef]
18. Islam, R.; Nasrin, S. Micropolar Fluid Flow Along with an Inclined Riga Plate Through a Porous Medium. *Int. J. Heat Technol.* **2021**, *39*, 1123–1133. [CrossRef]
19. Abbas, N.; Nadeem, S.; Malik, M. Theoretical study of micropolar hybrid nanofluid over Riga channel with slip conditions. *Phys. A Stat. Mech. Its Appl.* **2020**, *551*, 124083. [CrossRef]
20. Naseem, A.; Shafiq, A.; Zhao, L.; Farooq, M.U. Analytical investigation of third grade nanofluidic flow over a Riga plate using Cattaneo-Christov model. *Results Phys.* **2018**, *9*, 961–969. [CrossRef]
21. Khashi'Ie, N.S.; Arifin, N.; Pop, I. Mixed Convective Stagnation Point Flow towards a Vertical Riga Plate in Hybrid Cu-Al_2O_3/Water Nanofluid. *Mathematics* **2020**, *8*, 912. [CrossRef]
22. Chinyoka, T.; Goqo, S.; Olajuwon, B. Computational analysis of gravity driven flow of a variable viscosity viscoelastic fluid down an inclined plane. *Comput. Fluids* **2013**, *84*, 315–326. [CrossRef]
23. Nadeem, S.; Ahmed, Z.; Saleem, S. Carbon nanotubes effects in magneto nanofluid flow over a curved stretching surface with variable viscosity. *Microsyst. Technol.* **2019**, *25*, 2881–2888. [CrossRef]
24. Megahed, A.M.; Reddy, M.G. Numerical treatment for MHD viscoelastic fluid flow with variable fluid properties and viscous dissipation. *Indian J. Phys.* **2021**, *95*, 673–679. [CrossRef]
25. Mai-Duy, N.; Tanner, R. A spectral collocation method based on integrated Chebyshev polynomials for two-dimensional biharmonic boundary-value problems. *J. Comput. Appl. Math.* **2007**, *201*, 30–47. [CrossRef]
26. Khater, A.H.; Temsah, R.S. Numerical solutions of some nonlinear evolution equations by Chebyshev spectral collocation methods. *Int. J. Comput. Math.* **2007**, *84*, 305–316. [CrossRef]
27. Khater, A.; Temsah, R.; Hassan, M. A Chebyshev spectral collocation method for solving Burgers'-type equations. *J. Comput. Appl. Math.* **2008**, *222*, 333–350. [CrossRef]
28. Mai-Duy, N. An effective spectral collocation method for the direct solution of high-order ODEs. *Commun. Numer. Methods Eng.* **2005**, *22*, 627–642. [CrossRef]
29. Dehghan, M.; Fakhar-Izadi, F. The spectral collocation method with three different bases for solving a nonlinear partial differential equation arising in modeling of nonlinear waves. *Math. Comput. Model.* **2011**, *53*, 1865–1877. [CrossRef]